EAST EUROPEAN JOURNAL OF PHYSICS. 2. 138-149 (2023)
DOI:10.26565/2312-4334-2023-2-13 ISSN 2312-4334

ELECTROEXCITATION FORM FACTORS AND DEFORMATION OF ^{20,22}NE ISOTOPES BASED ON THE SHELL MODEL AND HARTREE-FOCK PLUS BCS CALCULATIONS[†]

Omar A. Alswaidawi, Ali A. Alzubadi
Department of Physics, College of Science, University of Baghdad, Baghdad, Iraq
Corresponding Author e-mail: ali.kareem@sc.uobaghdad.edu.iq
Received March 22, 2023; revised April 10, 2023; accepted April 11, 2023

Nuclear structure of ^{20,22}Ne isotopes has been studied via the shell model with Skyrme-Hartree-Fock calculations. In particular, the transitions to the low-lying positive and negative parity excited states have been investigated within three shell model spaces; *sd* for positive parity states, *spsdpf* large-basis (no-core), and *zbme* model spaces for negative parity states. Excitation energies, reduced transition probabilities, and elastic and inelastic form factors were estimated and compared to the available experimental data. Skyrme interaction was used to generate a one-body potential in the Hartree-Fock calculations for each selected excited state, which is then used to calculate the single-particle matrix elements. Skyrme interaction was used to calculate the radial wave functions of the single-particle matrix elements, from which a one-body potential in Hartree-Fock theory with SLy4 parametrization can be generated. Furthermore, we have explored the interplays among neutron and proton density profiles in two dimensions, along with the deformations of ^{20,22}Ne using Hartree-Fock plus BCS calculations.
Keywords: *Sd model space; negative parity state; elastic and inelastic form factor; density distribution*
PACS: 21.60.−n, 21.60.Cs, 21.10.−k

I. INTRODUCTION

For a microscopic description of the nucleus, different nuclear models have been utilized [1]. The most efficient one is the Shell Model (SM) [2], based on the idea of an independent nucleon freely orbiting in a spherically symmetrical core potential generated by all the other nucleons within the nucleus. In actual SM calculations, nuclear states are linear combinations of states rather than pure states [3]. Always, SM computations are performed in a configuration space with a limited number of single-particle states outside of an inert core, which is typically a doubly-magical nucleus. As a result of this truncation, the residual interactions must be regarded as effective interactions, and choosing the proper N-N interaction is not simple [4, 5]. The ground states of nuclei are created when nucleons fill shells to the Fermi level. Fermi's level is the same for protons and neutrons in stable nuclei, but the Coulomb repulsion between protons [6] explains why the line of stability and the N = Z line on the chart of the nuclides do not correspond for heavier nuclei. The laws of quantum mechanics govern the location and characteristics of the nucleus' discrete energy levels, just like they do for the atom. The positions of excited states vary from nucleus to nucleus. Excitation energy (E_x) is influenced by each nucleus's internal structure. Quantum numbers denote each excited state's angular momentum, parity, and isospin, in addition to its electromagnetic and strong properties. Positive-parity spectra can be generated by considering only the $1d_{5/2}$, $2s_{1/2}$, and $1d_{3/2}$ orbits in the *sd*-shell configuration space. Any realistic negative parity calculation must account for both $1p$ and $2p$-$1f$ active shells. In the absence of such theoretical work, approaches to comprehending the structure of negative-parity states typically rely on more generalized descriptions [7]. In a system of identical Fermions, the Pauli exclusion principle dictates that the properties of a nucleus with a given number of protons and neutrons are defined by the filling of the lowest energy single-particle levels (the nucleons in this case). The Pauli Exclusion Principle states that a particular set of quantum numbers can only be occupied by a single proton or neutron. The average nuclear potential is determined by the shape of the nuclear density distribution and the attractive short-range nucleon-nucleon interaction [8].

II. THEORETICAL FRAMEWORK

(a) Shell model calculations

The reduced matrix elements of the electron scattering $\hat{X}(\lambda)_{t_z}$ operator between the final f and initial i states can be expressed as the sum of the one-body density matrix (OBDM) times the reduced single-particle matrix elements [9];

$$\left\langle f \parallel \hat{X}(\lambda)_{t_z} \parallel i \right\rangle = \sum_{k_a k_b} \mathrm{OBDM}(fik_a k_b \lambda) \left\langle k_a \parallel \hat{X}(\lambda)_{t_z} \parallel k_b \right\rangle \tag{1}$$

The OBDM of multipolarity (λ) can be expressed in term of the second quantization notation as;

$$\mathrm{OBDM}(fik_{a,t_z} k_{b,t_z} \lambda) = \frac{\left\langle f \left\| \left[a^{+}_{k_a t_z} \otimes \tilde{a}_{k_b t_z} \right]^{\lambda} \right\| i \right\rangle}{\sqrt{2\lambda+1}} \tag{2}$$

[†] ***Cite as:*** O.A. Alswaidawi, and A.A. Alzubadi, East Eur. J. Phys. **2**, 138 (2023), https://doi.org/10.26565/2312-4334-2023-2-13

where the single-partical state (k), and t_z =1/2 and -1/2 for proton and neutron, respectively and i and f contain all the quantum numbers needed to separate the states.

M1 operator is used to define the nuclear magnetic dipole moment as [10]

$$\mu = \sqrt{\frac{4\pi}{3}} \begin{pmatrix} J_i & 1 & J_f \\ -J_i & 0 & J_f \end{pmatrix} \sum_{t_z} \left\langle f \left\| \hat{O}(M1)_{t_z} \right\| i \right\rangle \mu_N \tag{3}$$

where the nuclear magneton $\mu_N = \frac{e\hbar}{2m_p c} = 0.1051$ efm. While, in terms of the E2 operator, the electric quadrupole moment is defined as

$$Q = \sqrt{\frac{16\pi}{5}} \begin{pmatrix} J_i & 2 & J_f \\ -J_i & 0 & J_f \end{pmatrix} \sum_{t_z} \left\langle f \left\| \hat{O}(\mathrm{E2})_{t_z} \right\| i \right\rangle e_{t_z} \tag{4}$$

where the initial and final nuclear states |J> contain all the quantum numbers necessary to differentiate the nuclear states.

The reduced of transition probability given as [11].

$$B(X\lambda) = \frac{1}{4\pi} \left[Z \frac{(2\lambda+1)!!}{k^{\lambda}} \right]^2 \; |F(X\lambda,k)|^2 \tag{5}$$

where $k = E_X/\hbar c$, $B(E\lambda)$ is in unit of $e^2fm^{2\lambda}$ and $B(M\lambda)$ is in the unit of $\mu_N{}^2\, fm^{2\lambda-2}$.

With the realization that the energy functional could be written as a zero-range expansion, the Skyrme interaction was developed for nuclear structure computations, resulting in a straightforward derivation of the Hartree-Fock (HF) equations in which exchange terms have the same mathematical structure as direct terms. This approach decreases significantly the number of single-particle state integrations necessary to solve the equations. The Skyrme energy (E_{Sky}) reflects the strong force in the particle-hole channel in coordinate space and consists of central, spin-orbit, and tensor contributions [6]. Central potential is represented by Skyrme potential. It is a one-body potential as a mean-field potential.It is designed to approach the realistic nucleon–nucleon forces by providing the average field owing to all of the nucleons constituting the nucleus. VSky equals the combination of two and three bodily components. [12] as:

$$\hat{V}_{Sky} = \sum_{i<j} V_{ij}^{(2)} + \sum_{i<j<k} V_{ijk}^{(3)} \tag{6}$$

The two-body part is given by:

$$\begin{aligned} \hat{V}_{Sky}^{(2)}(i,j) = \; & t_0(1+x_0\hat{P}_\sigma)\delta_{12} + \frac{t_1}{2}(1+x_1\hat{P}_\sigma)\left[\vec{k}'^2\delta_{12} + \delta_{12}\vec{k}^2\right] \\ & + t_2(1+x_2\hat{P}_\sigma)\vec{k}'\delta_{12}\vec{k} + \frac{t_3}{6}(1+x_3\hat{P}_\sigma)\rho\left(\frac{\vec{r}_1+\vec{r}_2}{2}\right)^{\alpha}\delta_{12} + \; iW_0 \; \vec{k}'\delta_{12}(\vec{\hat{\sigma}}_1+\vec{\hat{\sigma}}_2)\times\vec{k} \\ & + \frac{t_e}{2}\left(\left[3\,(\vec{\hat{\sigma}}_1\cdot\vec{k}')\,(\vec{\hat{\sigma}}_2\cdot\vec{k}') - (\vec{\hat{\sigma}}_1\cdot\vec{\hat{\sigma}}_2)\vec{k}'^2\right]\delta_{12} + \delta_{12}\left[3(\vec{\hat{\sigma}}_1\cdot\vec{k})\,(\vec{\hat{\sigma}}_2\cdot\vec{k}) - (\vec{\hat{\sigma}}_1\cdot\vec{\hat{\sigma}}_2)\vec{k}^2\right]\right) \\ & + t_0\left[3(\vec{\hat{\sigma}}_1\cdot\vec{k})\delta_{12}(\vec{\hat{\sigma}}_2\cdot\vec{k}) - (\vec{\hat{\sigma}}_1\cdot\vec{\hat{\sigma}}_2)\vec{k}'\delta_{12}\vec{k}\right] \end{aligned} \tag{7}$$

where $\delta_{12} = \delta(\vec{r}_1 - \vec{r}_2)$, The $\hat{k}$ and $\hat{k}'$ operators represent the relative wave vectors of two nucleons acting to the right and left, respectively (i.e., complex conjugate wave functions with coordinate r'), They possess the shape;

$$\hat{K} = \frac{1}{2i}(\vec{\nabla}_1 - \vec{\nabla}_2) \;\; \text{and} \;\; \hat{K}' = -\frac{1}{2i}(\vec{\nabla}_1 - \vec{\nabla}_2) \tag{8}$$

Also

$$\hat{P}_\sigma = \frac{1}{2}(1+\hat{\sigma}_1.\hat{\sigma}_2) \tag{9}$$

Electron scattering form factor between final and initial nuclear shell model states, including angular momentum λ and momentum transfer q, is given by [13].

$$\left|F_\lambda^\chi(q)\right|^2 = \left(\frac{4\pi}{Z^2}\right)\frac{1}{(2J_i+1)}\left|\sum_{t_z} e(t_z)\left\langle J_f \left\| \hat{T}_{\lambda,t_z}^{\chi}(q) \right\| J_i \right\rangle F_{cm}(q)F_{fs}(q)\right|^2 \tag{10}$$

where J_f and J_i are the total angular momentum λ of final and initial state, F_{cm} (q) is the correction (center- of-mass) and $F_{fs}(q)$ is the finite size of the nucleon, with χ involving the transverse (T) and longitudinal (C) form factors. The nuclear

structure enters into the electron scattering through the longitudinal F^C form factor and the transverse F^T form factors (F^E and F^M) are the electric and magnetic transverse form factor, respectively). The total longitudinal and transverse form factors for electron scattering are given by:

$$\left|F^C(q)\right|^2 = \sum_{J\geq 0}\left|F_\lambda^C(q)\right|^2 \tag{11}$$

$$\left|F^T(q)\right|^2 = \sum_{J>0}\left[\left|F_\lambda^E(q)\right|^2 + \left|F_\lambda^M(q)\right|^2\right] \tag{12}$$

These form factors are functions of the momentum transfer q only.

$$\left|F_\lambda^C(q)\right|^2 = \frac{4\pi}{Z^2(2J_i+1)}\left|\left\langle Jf\left\|M_\lambda^C\right\|J_i\right\rangle\right|^2 \tag{13}$$

$$\left|F_\lambda^E(q)\right|^2 = \frac{4\pi}{Z^2(2J_i+1)}\left|\left\langle Jf\left\|T_\lambda^e\right\|J_i\right\rangle\right|^2 \tag{14}$$

$$\left|F_\lambda^M(q)\right|^2 = \frac{4\pi}{Z^2(2J_i+1)}\left|\left\langle Jf\left\|T_\lambda^m\right\|J_i\right\rangle\right|^2 \tag{15}$$

The related to the electromagnetic transition operators as

$$(M_\lambda^C,\ T_\lambda^e,\ T_\lambda^m)$$

$$M_{\lambda_\mu}^C(q) = \int d^3r\, j_\lambda(qr)Y_{\lambda_\mu}\hat{\rho}(r) \tag{16}$$

$$T_{\lambda_\mu}^e(q) = \frac{1}{q}\int d^3r\left\{\nabla\times j_\lambda(qr)Y_{\lambda\lambda 1}^\mu\right\}.\hat{J}(r) + q^2\int d^3r\left\{j_\lambda(qr)Y_{\lambda\lambda 1}^\mu\right\}.\hat{\mu}(r) \tag{17}$$

$$T_{\lambda_\mu}^m(q) = \int d^3r\left\{j_\lambda(qr)Y_{\lambda\lambda 1}^\mu\right\}.\hat{J}(r) + \int d^3r\left\{\nabla\times j_\lambda(qr)Y_{\lambda\lambda 1}^\mu\right\}.\hat{\mu}(r) \tag{18}$$

where $\hat{\rho}(r)$, $\hat{J}(r)$, and $\hat{\mu}(r)$, are the nuclear charge, the magnetization current density operators is $j_\lambda(qr)$, Bessel function of order λ, $Y_{\lambda\mu}$ is the spherical harmonic. The total form factor is equal to the addition of the longitudinal and transverse relations:

$$\left|F(q)\right|^2 = \left|F_\lambda^C(q,f,i)\right|^2 + \left(\frac{1}{2}+\tan^2(\frac{\theta}{2})\right)\left|F_\lambda^T(q,f,i)\right|^2 \tag{19}$$

(b) Hartree-Fock plus BCS calculations

The self-consistent mean field based on HF plus BCS calculations are designed to describe the structure of nuclei and study the evolution shapes, using the Skyrme forces performed to study the transitional in density shape where the pairing correlation have been taken into account. HF method is probably the best method for anticipating the total binding energies and single particle energies of closed shell nuclei [14]. Also SHF is a useful tool because this force is central and has zero-range interactions [15]. Nuclei is a quantum many-body system exhibiting the quadrupole collectivity associated with the shape of the mean field. The collective degree of freedom is associated with the measure of the operator $\hat{Q}$.

From these single-particle wave functions and fractional occupation amplitudes, a mean-field theory can be built υ_α, i.e., [16]

$$\{\psi_\alpha, \upsilon_\alpha, \alpha = 1,...,\Omega\} \tag{20}$$

where Ω denotes the size of the active single particle space.

The formula for the resulting BCS many-body state is [16].

$$|\phi\rangle = \prod_{\alpha>0}\left(u_\alpha + \upsilon_\alpha\hat{a}_\alpha^+\hat{a}_{\bar{\alpha}}^+\right)|0\rangle \tag{21}$$

Where $|0\rangle$ is the particle-vacuum state, is the Fermion production operator $\hat{a}_\alpha^+$ in state ψ_α, and is the time-reversed partner to state α. The local density of nucleons is defined as [16]

$$\rho_q(\vec{r}) = \sum_{\alpha\in q}\sum_s \upsilon_\alpha^2\left|\psi_\alpha(\vec{r},s)\right|^2 \tag{22}$$

The local nucleon density is defined as [16]

$$\rho_q(\vec{r}) = \sum_{\alpha \in q} \sum_{s} \upsilon_\alpha^2 \left|\psi_\alpha(\vec{r},s)\right|^2 \tag{23}$$

The total energy consists of

$$E_{tot} = T + E_{Skyrme} + E_{Coulomb} + E_{pair} + E_{cm} \tag{24}$$

$$E_C = \frac{e^2}{2}\int dV dV' \frac{\rho_p(\vec{r})\rho_p(\vec{r}')}{|\vec{r}-\vec{r}'|} - \int dV \frac{3e^2}{4}\left(\frac{3}{\pi}\right)^{\frac{1}{3}} \rho_p^{4/3} \tag{25}$$

where E_{Culomb} is the Coulomb energy

$$E_{pair} = \frac{1}{4} \sum_{q \in \{p,n\}} V_{pair,q} \int dV \left|\xi_q\right|^2 \left[1 - \frac{\rho}{\rho_{0,pair}}\right] \tag{26}$$

the pairing energy is

$$\xi_q(\vec{r}) = \sum_{\alpha \in q} \sum_{s} w_\alpha u_\alpha \upsilon_\alpha \psi_{\bar{\alpha}}(\vec{r},s)\psi_\alpha(\vec{r},s) \tag{27}$$

where dV represents the volume element in whole three-dimensional space and is the fundamental charge e. with e^2=1.43989 MeV.fm, and ξ_q is the pairing density, w_α is a soft pairing space cut-off. The variables $s \in \pm 1$ represent the spinor component of the wave functions.

The pairing energy includes the parameter $\rho_{0,pair}$ that controls the equilibrium between volume and surface pairing. Deformation of the nucleus is defined as the departure from spherical symmetry about the center of mass (c.m), which is quantified by the electric quadrupole moment. Hence, the most significant moments are center-of-mass moments [16]

$$\vec{R}_{type} = \frac{\int dV\, \vec{r}\, \rho_{type}(\vec{r})}{\int dV\, \rho_{type}(\vec{r})} \tag{28}$$

In terms of the spherical quadrupole moments, the anisotropic combinations can be quantified

$$Q_{2m,type} = \int dV\, r^2\, Y_{2m}\, \rho_{type}\left(\vec{r} - \vec{R}_{type}\right) \tag{29}$$

the quadrupole deformation parameter

$$\beta_{20} = \frac{4\pi}{3}\frac{Q_{20}}{AR^2}\ ,\ R = R_0\, A^{1/3}\ \ ,\ R_0 = 1.2\ \text{fm} \tag{30}$$

III. RESULTS AND DISCUSSION

In this study, the OBDM elements for low-lying positive parity J^+ states were calculated using the *sd*-shell model space. For negative parity J^- states, the *spsdpf* no core with (0, 1) ħω restriction and the *zbme* shell model spaces have been employed. Using the NuShellX@MSU code [17], all calculations were performed. As we mentioned previously, the Skyrme interaction was used to calculate the radial wave functions of the single-particle matrix elements, from which a one-body potential in HF theory with SLy4, parametrization can be generated in addition to the harmonic oscillator (HO) and Wood-Saxson potentials. For ^{20,22}Ne isotopes, using USDC [18] two-body effective interaction in the calculation of the OBDM and SLy4 parameterization yields root mean square (rms) charge radii of 2.954 and 2.9525 *fm*, which are in good agreement with the experimental values 3.005 and 2.9525 *fm* [19]. The calculated binding energies are 150.15 and 168.84 MeV, which are in reasonable agreement with the experimental values of 160.64 and 177.76 MeV [20]. The nuclear magnetic dipole moment is (1.076 and 0.780) *nm*, in good agreement with experimental values of +1.08 and +0.65 *nm* [19], and the electric quadrupole moment (Q2) is -14.31, and -14.03 $e^2.fm^2$, the experimental -23(3), -19(4) $e^2.fm^2$ [19]. All these results together match the experimental value.

Also, we have used the code SkyAx [16] is a highly optimized two-dimensional HF+ Bardeen-Cooper-Schrieffer (BCS) code is using for computing ground states and deformation energy surfaces for axially symmetric deformed nuclei. The calculated results will be discussed in three sections. The first will focus on the Excitation Energies and reduce transition probability, the second on electroexcitation Form Factor, and the third on structure densities in two dimensions (Contour Lines), which will be given.

1. Excitation Energies and reduce transition probability

The excitation energies and reduced transition probabilities for low-lying positive and negative parity states in ^{20,22}Ne isotopes are calculated and tabulated in Table 1 and compared with the corresponding experimental data. The OBDM

elements for positive parity states were calculated using *sd* MS with the last updated two-body effective interactions USDE [21] and USDC [18]. In contrast, for negative ones, we have used the *spsdpf* (no core with one ħω restriction) and *zbme* model spaces with WBP and REWILE effective interactions, respectively.

The majority of estimated excitation energies in all model spaces closely match experimental data. [19], except for a few levels. Those levels with deviations exceeding 1.5 MeV include 2_3^+ at 7.833 MeV for ^{20}Ne and 4_2^+ at 6.345 MeV for ^{22}Ne. The negative-parity energy levels are accurately predicted using *zbme* MS. However, for *spsdpf* MS, the excitation energy state 1_1^- at 7.119 MeV is overestimated by the experimental data. The coupling between the states, such as the $1p_{1/2}$ holes coupled to the $1d_{5/2}$ neutron ($1p$-$1h$), may account for these discrepancies. The additional pairing correlation and a change in the proton–neutron interaction, which results in a more considerable quadrupole deformation energy, reduce the energy of the $1p$–$1h$ state [8]. Fig.1 illustrates the extent of convergence between theoretical calculations and experimental data.

The calculated reduced transition probabilities $B(EL)$ for the low-lying positive and negative parity states in ^{20}Ne and ^{22}Ne isotopes are presented in Table 2. The discrepancies with experimental data regarding the energy of transitions from these states might be due to the possible admixture of states involving neutron and proton excitations. From a general point of view, the $B(EL)$ values for the transitions of low excitation energies agree reasonably well with experimental data [20,22-24]. The $B(E2)$ transition rates are slightly larger than the experimental data except for 2_1^+, where the agreement is quite good for 2_3^+ in ^{22}Ne using the USDE interaction. The slight difference between the experimental data and the theory could be because the quadrupole vibration was not taken into account. Regarding $B(E3)$ and $B(E1)$ transition probabilities in ^{22}Ne, the calculated results are in poor agreement with the experimental results.

Table 1. Excitation energies in MeV for a different transition to excited states using two-body interactions USDE, USDC, WBP, and REWILE. The experimental data taken from Ref. [19]

Nucleus	J^π	E_x(Exp.)	Model Space			
			sd		*spsdpf*	*zbme*
			USDE	USDC	WBP	REWILE
^{20}Ne	2_1^+	1.633(15)	1.736	1.735	---	---
	2_2^+	7.421(12)	7.548	7.532	---	---
	2_3^+	7.833(15)	9.598	9.992	---	---
	4_1^+	4.247(11)	4.192	4.146	---	---
	4_2^+	9.031(7)	9.974	9.956	---	---
	3_1^-	5.787(26)	---	---	7.119	6.099
	1_1^-	5.621(17)	---	---	5.448	5.436
^{22}Ne	2_1^+	1.274(7)	1.350	1.345	---	---
	2_2^+	4.456(9)	4.301	4.321	---	---
	2_3^+	5.363(11)	5.160	5.130	---	---
	4_1^+	3.357(5)	3.370	3.335	---	---
	4_2^+	6.345(10)	5.380	5.404	---	---
	3_1^-	5.910(9)	---	---	5.372	5.386
	1_1^-	6.689(11)	---	---	6.671	5.720

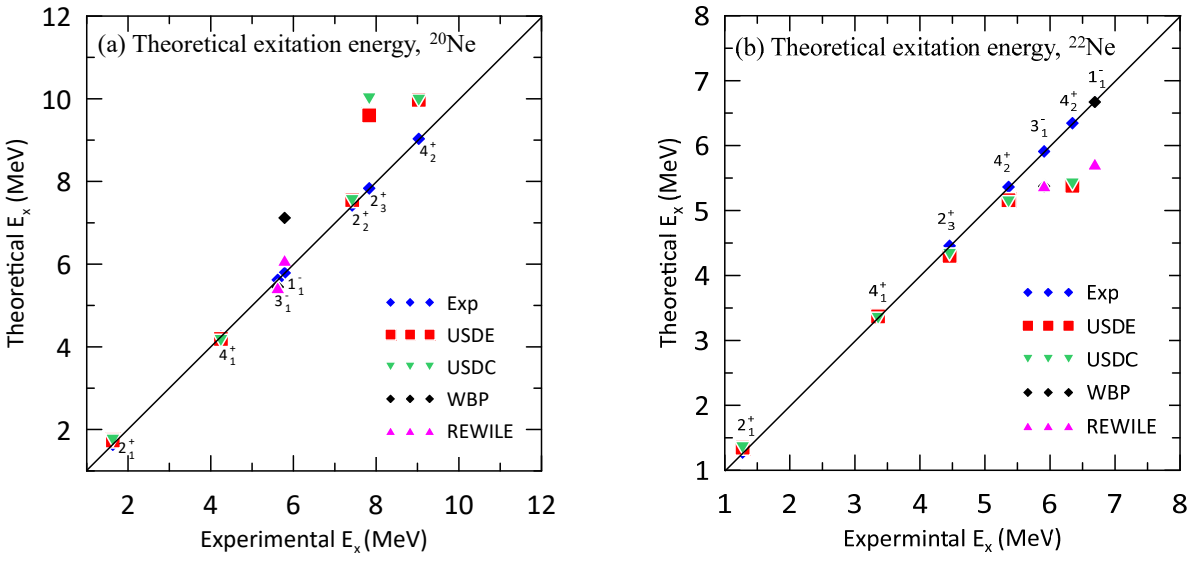

Figure 1. Theoretical excitation energies in MeV states vs. experimental for the different transition to low-lying excited states using USDE, WBP, and REWILE two-body effective interactions. The experimental data are taken from Ref. [19].

Table 2. The reduced transition probabilities B(EL) in e^2fm^{2L} for the different transition to excited states using two-body interactions USDE, USDC, WBP, and REWILE. The experimental data taken from Ref. [20, 22-24]

Nucleus	J^π	E_x(Exp.)	B (EL)Exp	B(EL)Theo.	
				USDE	USDC
^{20}Ne	2_1^+	1.633(*15*)	340(30)	462	247.1
	2_2^+	7.421(12)	0.13(0.03)	0.185	0.112
	2_3^+	7.833(15)	0.83(0.13)	2.901	2.474
	4_1^+	4.247(11)	---	0.6257E+05	0.6408E+05
	4_2^+	9.031(7)	---	0.3418E+04	0.3548E+04
				WBP	**REWILE**
	3_1^-	5.787(26)	1763	2172	1528
	1_1^-	5.621(17)	---	0.187E-03	0.252E-07
				USDE	**USDC**
^{22}Ne	2_1^+	1.274(7)	271(36)	384	393
	2_2^+	4.456(9)	13(2)	31.1	29.5
	2_3^+	5.363(11)	3.2(1.5)	3.802	2.48
	4_1^+	3.357(5)	17000(4000)	20500	21930
	4_2^+	6.345(10)	---	7076	6904
				WBP	**REWILE**
	3_1^-	5.910(9)	870(250)	407.7	1278
	1_1^-	6.689(11)	0.08(0.04)	0.914 E-05	0.349 E-03

2. Electroexcitation form factor

The nuclear structure can only enter the cross-section through longitudinal (FC), transverse (FE), and magnetic (FM). These form factors are functions of the momentum transfer q only. The FC and FT form factors correspond to fields parallel and perpendicular to the direction of momentum transfer, respectively [25]. $|F_T(q)|^2$, is influenced by both magnetic and electric currents, whereas $|F_L(q)|^2$ is caused solely by the electric Coulomb field.

A. Elastic electron scattering form factor ($J^\pi = 0^+$)

Fig. 2 (a) and (b) depicts the calculated elastic longitudinal C0 electroexcitation form factors for the ground state (GS) of ^{20,22}Ne isotopes in the *sd*-shell MS wave functions employing SLy4, HO, and WS parameterization compared with experimental data from Ref. [22,26]. Observable agreement exists in the momentum transfer region of q (0-1.3) fm^{-1}, based on experimental data.

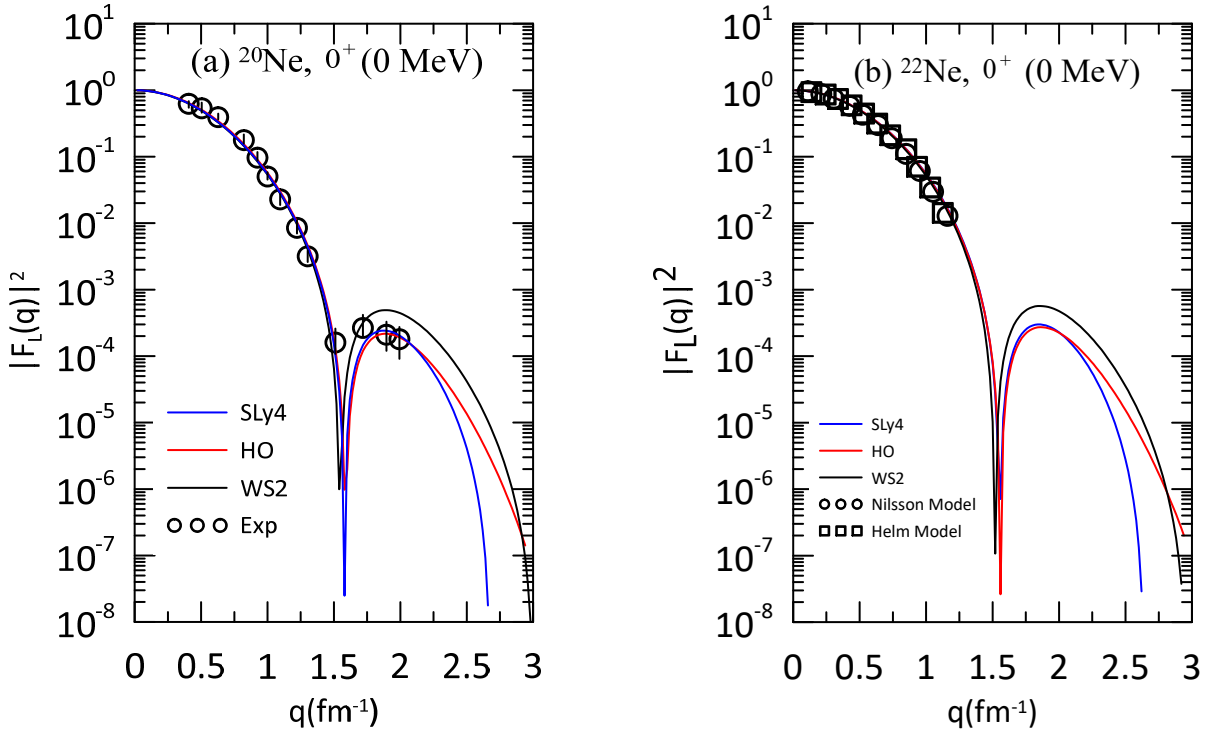

Figure 2. Theoretical longitudinal C0 form factors (a) for ^{20}Ne isotope 0^+, (0 MeV) (b) for ^{22}Ne isotope 0^+, (0 MeV) using SLy4 parameterization, HO and WS compared with experimental data taken from Ref [22, 23]

B. Inelastic scattering form factor

1. Positive parity states

The calculated inelastic longitudinal C2 electroexcition form factors of transition at positive parity states 2^+ in ^{20}Ne isotope are shown in Fig. 3; (a) 2_1^+(1.633 MeV), (b) 2_2^+(7.422 MeV), and (c) 2_3^+(7.833 MeV), and for ^{22}Ne isotope Fig.4 (a) 2_1^+(1.274 MeV), (b) 2_2^+(4.456 MeV), and (c) 2_3^+(5.363 MeV). Inspection of these figures reveals that the longitudinal form factors are all dominated by the electric quadrupole transition C2 components and are in reasonable agreement with available experimental data [22,23] using all the single particle potentials. Although we have not been changing parameters, they were altered to accommodate the experimental electron scattering data. The WS potential agrees satisfactorily with experimental data, except 2_2^+, at (7.422MeV) higher than experimental data at all momentum transfer points.

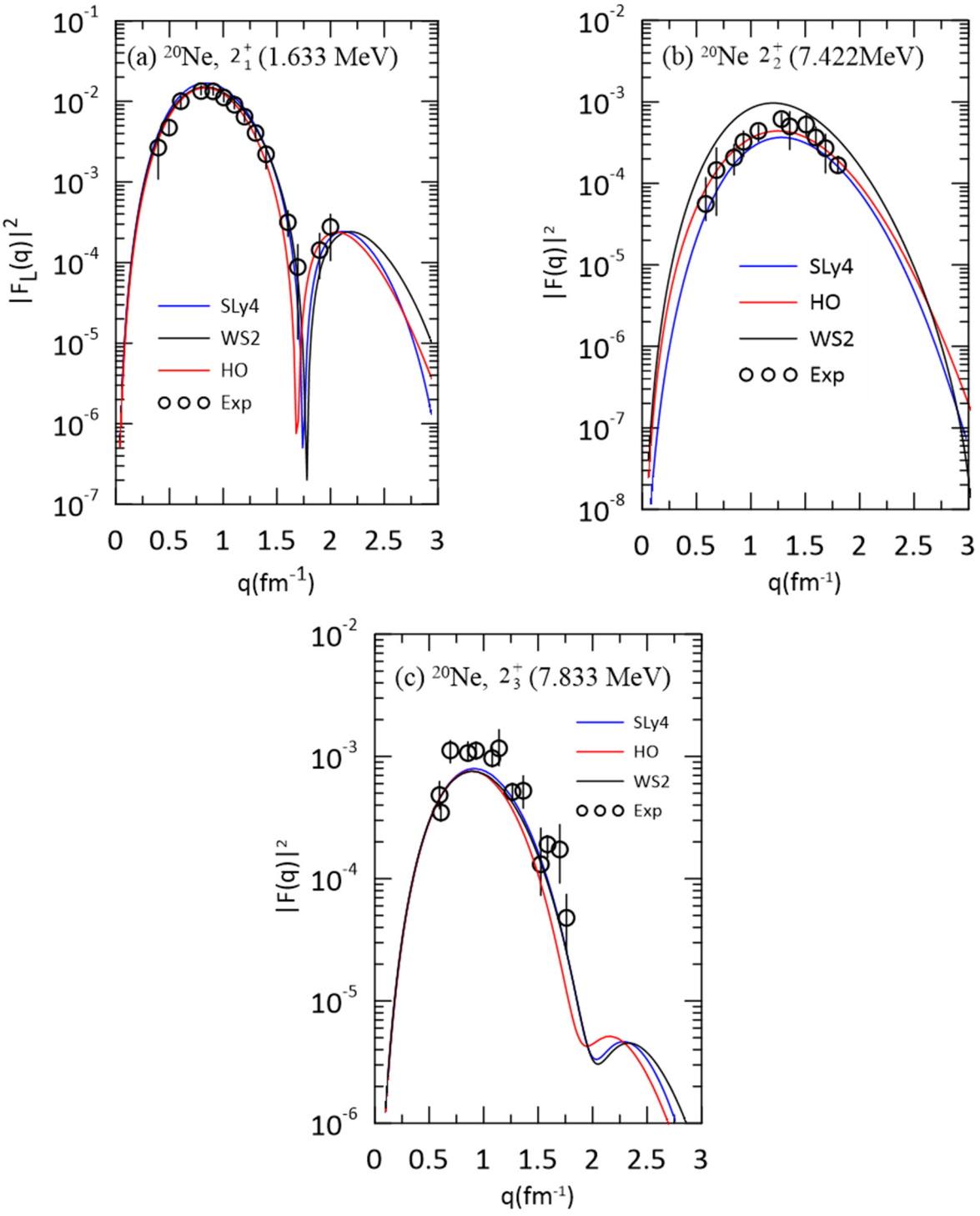

Figure 3. longitudinal C2 form factor for ^{20}Ne using SLy4, HO, and WS parametrizations vs with the experimental value taken from Ref. [22,23]

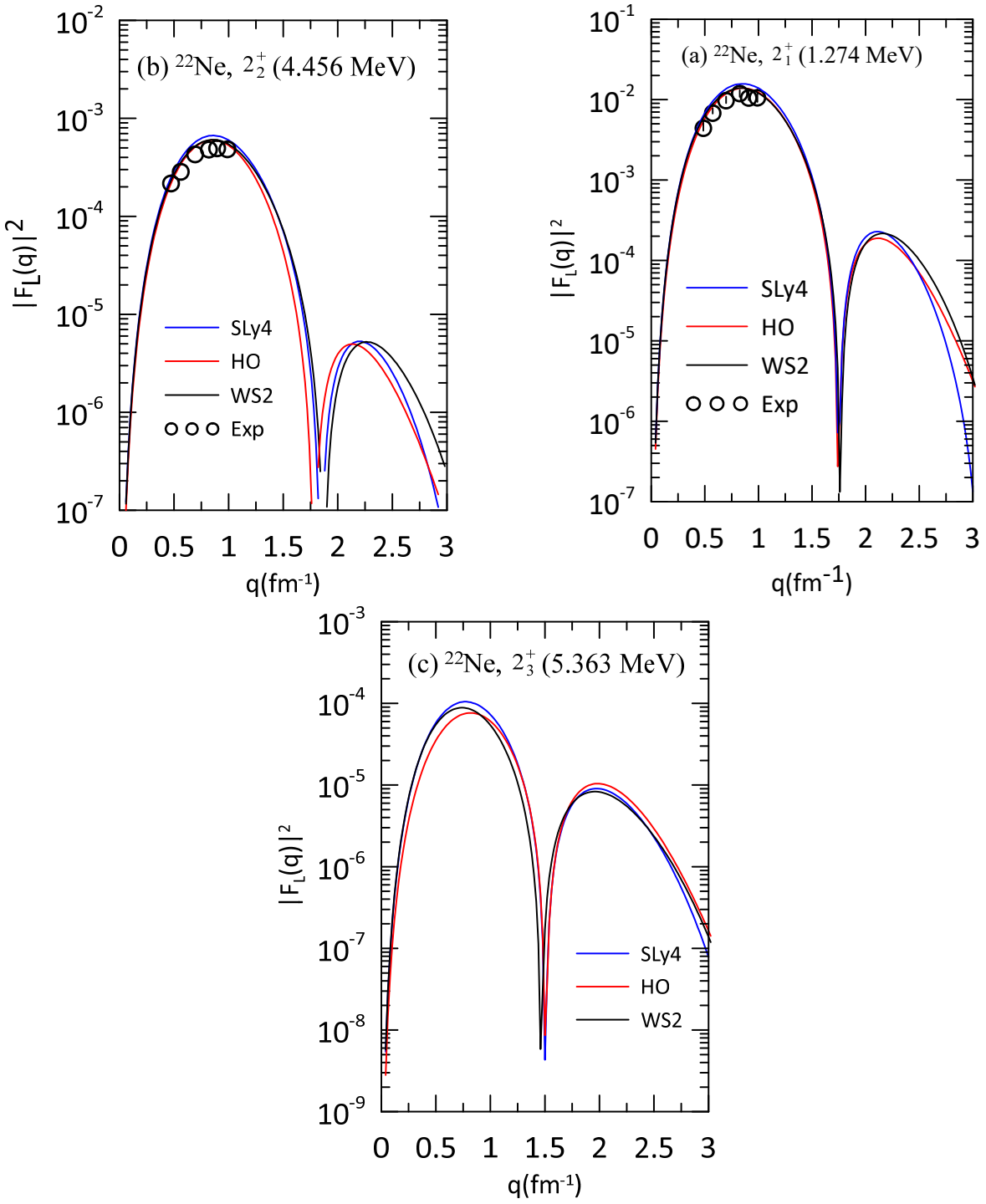

Figure 4. longitudinal C2 form factor for ^{22}Ne calculate by SLy4, HO, and WS parametrizations vs the experimental data taken from Ref. [22,23].

Fig. 5 (a) and (b) show the calculated inelastic longitudinal C4 electroexcitation form factor of the transition to the 4^+ state in ^{20}Ne at (4.2477MeV) and in ^{22}Ne at (3.357 MeV). It is obvious that the longitudinal form factor is dominated by electric hexa transition C4 components and in reasonable agreement with experimental data in light of the fact that parameters were not changed to fit the experimental electron scattering data [23,24].

2. Negative parity states

Based on the results obtained in showing the sensitivity of the effect of changing the single particle potentials. The longitudinal form factors were calculated, considering the effect of the two-particle interactions in improving the convergence with the practical values. Fig. 6 shows the calculated total form factors for the transition to the negative-parity state1_1^-, (5.787 MeV) and 3_1^-, (5.624 MeV) for ^{20}Ne isotope compared with experimental data [23], which refer to the total sum of (1_1^- ,3_1^-) states together. The WBP interaction predicts a rapid increase in low-lying C3 concentration.

While C1 form factor result under the experimental data. On the contrary, the REWILE result is in reasonable agreement with experimental results for the C3 form factor, in contrast to the C1 result, which was based on experimental data.

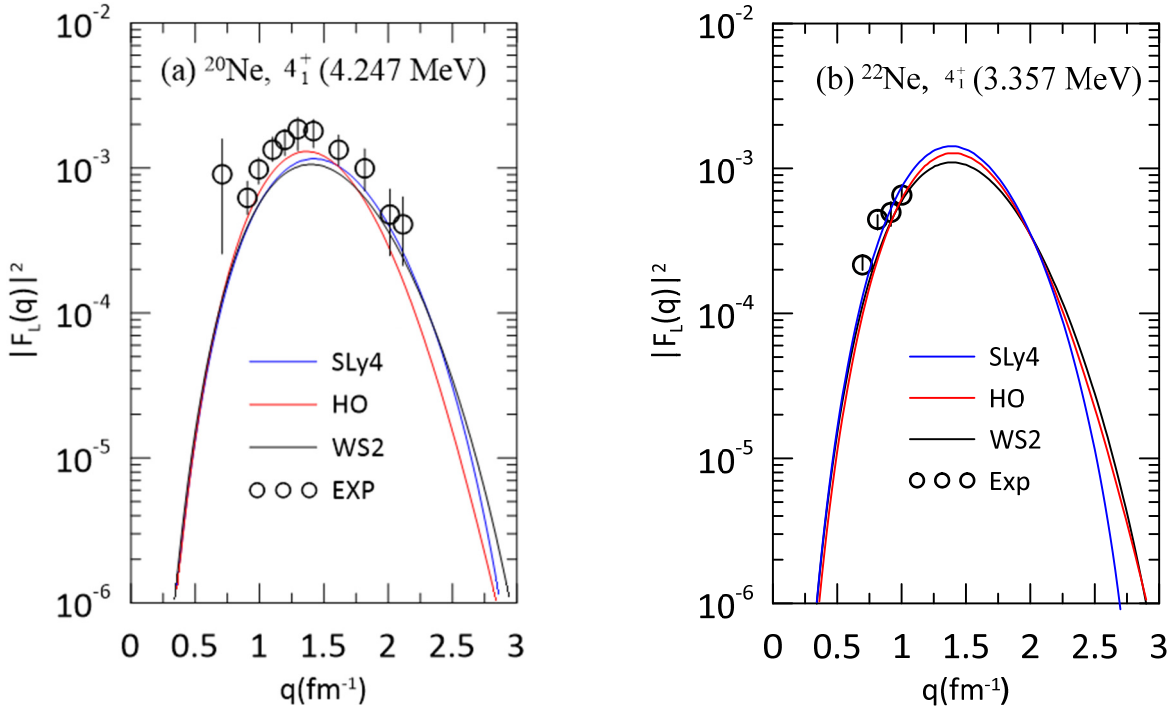

Figure 5. Theoretical longitudinal C4 form factor for ^{20}Ne and ^{22}Ne isotope, using SLy4 parameterization in comparison with experimental data taken from Ref. [23, 24].

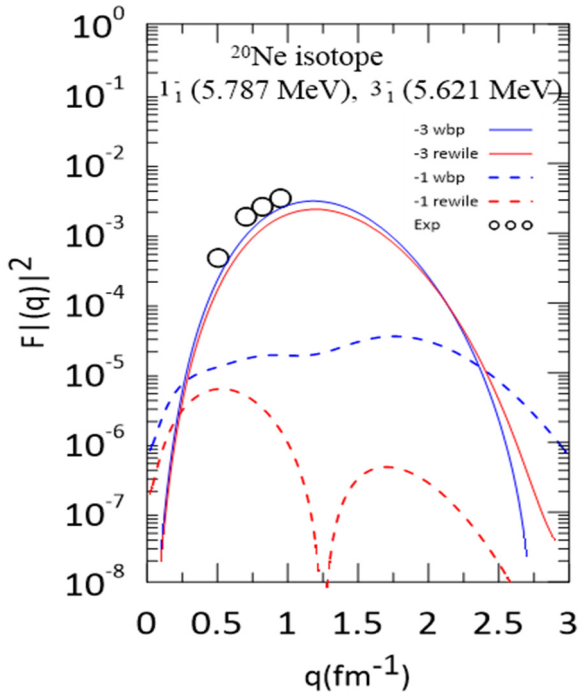

Figure 6. Total form factor for the transition $^{-}1_1$(5.578) and $^{-}3_1$(5.621MeV) using SLy4 parameterization in comparison with experimental data taken from Ref [26]

Fig. 7 (a), and (b) show the calculated longitudinal C1, C3 form factors in ^{22}Ne isotope for the transitions 1_1^-, (6.689 MeV) and 3_1^-, (5.910 MeV) states. The WBP prediction agrees qualitatively with experimental data in all momentum transfer regions of these data. Also, it can be observed that the REWILE prediction for the longitudinal C1 form factors under estimate the experimental result. The longitudinal C1 experimental data reveals an additional maximum form factor. The theoretical C1 contribution does not include this maximum. From the our previous calculates

we noted that WBP is the best in approximation with experimental data, thus means the contribution valance nucleon in $1p_{3/2}$ state is accountable for the substantial C1, C3 strength.

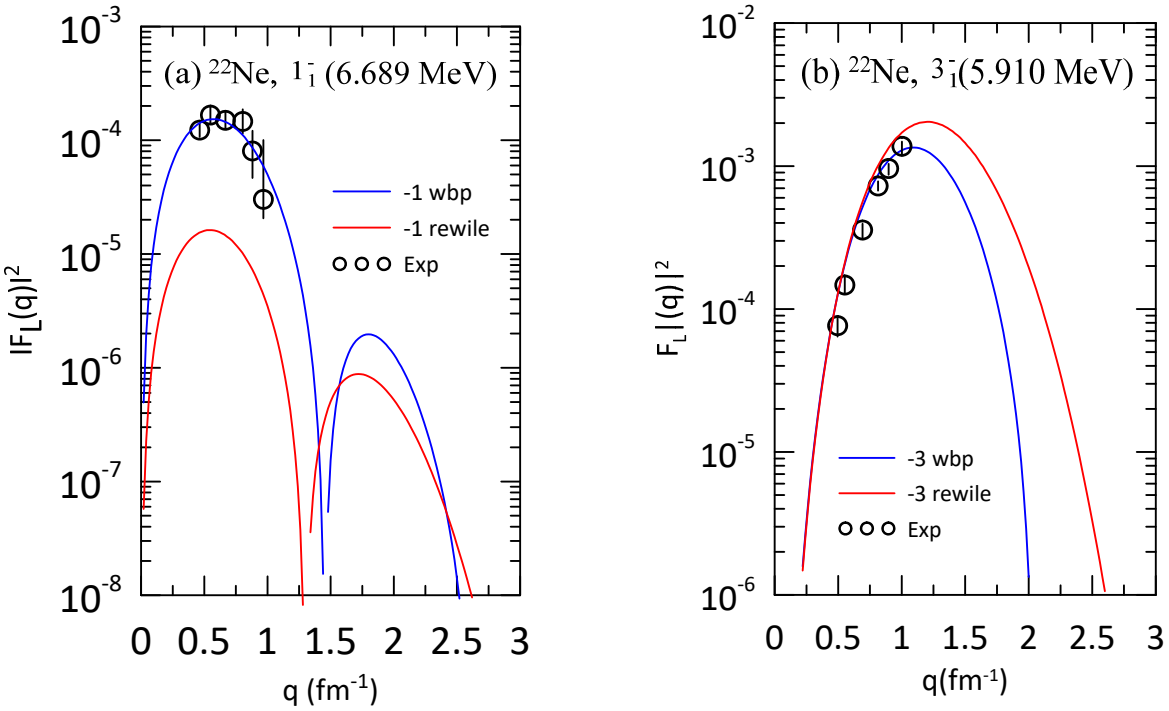

Figure 7. Theoretical longitudinal C1 and C3 form factor (a) for1^-_1, 6.689 MeV. (b) For 3^-_1, 5.910 MeV using SLy4 parameterization in comparison with experimental data taken from Ref. [23]

3. The Quadrupole Deformation using BCS Calculation

Fig. 8 and 9 shows the potential energy curve of $^{20,\ 22}$Ne isotopes (on the left) as a function of the quadrupole deformation parameter $\beta 2$. The corresponding neutron and proton structure densities are also displayed (on the right). Following the color code, the red and blue colors correspond to the high density (~0.08 fm^{-3}) and low density (~0.02 fm^{-3}), respectively. The two local minima in Fig. 8 are predicted as (a) β_2=-0.154 and (b) β_2=0.406. ^{20}*Ne* have a stable quadrupole deformation where the high neutron and proton density distribution is in the center for the two regions (a) and (b), as expected (^{20}Ne have the same numbers of protons and neutrons), where there is no effect of *n-p* pairing. For the ^{22}Ne isotope, the two local minima in Fig. 9 are predicted as (a) β_2=-0.204 and (b) β_2=0.404. We can notice that the stability decreases with decreasing central proton density because of the two neutrons added to the last state, which increases the effect of *n-p* pairing.

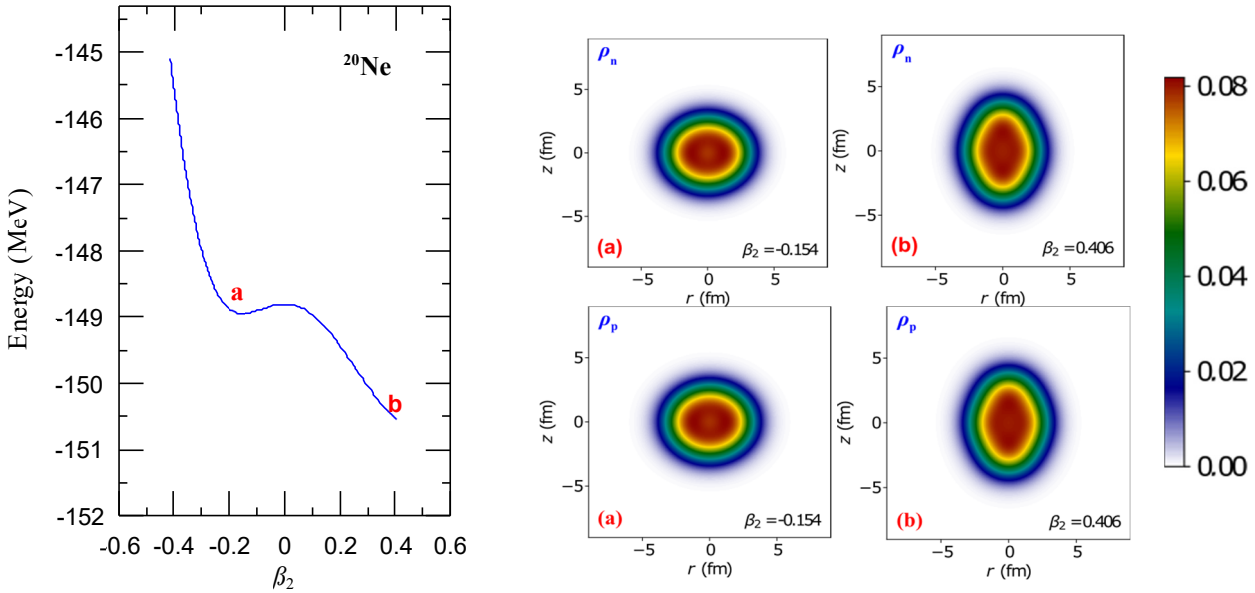

Figure 8. Left, the potential energy curve of ^{20}*Ne* as a function of the quadrupole deformation parameter. The neutron and proton structure densities corresponding to the two local minima, marked a, and b are shown in the right panel

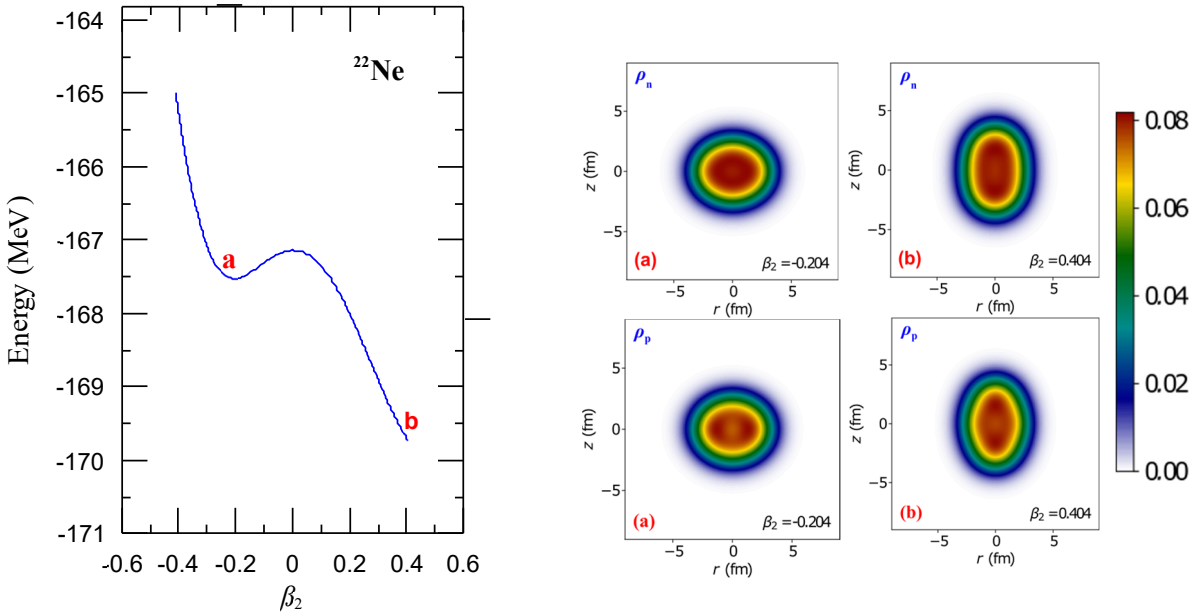

Figure 9. Left, the potential energy curve of ^{22}Ne as a function of the quadrupole deformation parameter. The neutron and proton structure densities corresponding to the two local minima, marked a, and b are shown in the right panel

IV. CONCLUSION

In this study, the nuclear structure of ^{20,22}Ne isotopes was investigated in the framework of the shell model and BCS calculation with Skyrme parametrization. In this context, excitation energies and the corresponding reduced transition probabilities, the elastic and inelastic electroexcitation form factors for positive and negative parity states in the momentum-transfer range 0.0 <q< 3.0 fm^{-1}, and quadrupole deformation parameter are discussed. Additionally, the work inspects the effect of three single-particle potentials; in particular, HO, WS and SLy4 parameterizations. It can be concluded that, on the whole, the impression of using different model spaces has fairly well reproduced the experimental data for positive and negative parity states and is not sensitive for changing the single particle potentials rather than the two-body effective interactions. The most important limitation lies in the fact that the strong collective feature of the nuclei in this mass region and internally consistent interaction formulation.

ORCID IDs

Ali A. Alzubadi, https://orcid.org/0000-0002-7226-1141

REFERENCES

[1] R. Stock, *Encyclopedia of Nuclear Physics, and its Applications*, 1st edition, (Wiley-VCH, 2013).
[2] O. Sorlin, and M.G. Porquet, "Nuclear magic numbers: new features far from stability," Prog. Part. Nucl. Phys, **61**, 602-673 (2008). https://doi.org/10.1016/j.ppnp.2008.05.001
[3] R.F. Casten, *Nuclear Structure from a Simple Perspective*, 2nd edition, (Oxford Univ. Press, New York, 2000).
[4] P. Ring, and P. Schuck, *The Nuclear Many-Body Problem*, (Springer Verlag, Berlin Heidelberg, 1980).
[5] E. Caurier, G. Martinez-Pinedo, F. Nowacki, A. Poves, and A.P. Zuker, Rev. Mod. Phys. **77**, 427 (2005). https://dx.doi.org/10.1103/RevModPhys.77.427
[6] W. Greiner, and J.A. Maruhn, *Nuclear Models*, (Springer, 1996).
[7] J.B. Mc.Grory, and B.H. Wildenthal, Phys. Rev. C, **7**, 974 (1973). https://doi.org/10.1103/PhysRevC.7.974
[8] J.E. Garcia-Ramos, M.V. Andrés, J.A.L. Valera, and A.M. Moro, editors, *Basic Concepts in Nuclear Physics: Theory, Experiments and Applications*, (Springer, Span, 2018). https://doi.org/10.1007/978-3-030-22204-8
[9] R.A. Radhi, A.A. Alzubadi and A.H. Ali, Phys. Rev. C, **97**, 064312 (2018). https://doi.org/10.1103/PhysRevC.97.064312
[10] P.J. Brussaard, and P.W.M. Glaudemans, *Shell Model Appli ations in Nuclear Spectroscopy*, (North Holand, Amsterdam, 1977).
[11] R.A. Radhi, A.A. Alzubadi, and N.S. Manie, Phys. Rev. C, **97**, 1 (2018). https://doi.org/10.1103/PhysRevC.97.024316
[12] D. Vautherin, and D.M. Brink, Phys. Rev. C, **5**, 626 (1972). https://doi.org/10.1103/PhysRevC.5.626
[13] T. de Forest, and J.D. Walecka, Adv. Phys. **15**, 1 (1966). https://doi.org/10.1080/00018736600101254
[14] A.A. Alzubadi, and R.A. Allawi, Indian J. Phys. **96**, 1205 (2022). https://doi.org/10.1007/s12648-021-02052-x
[15] A.A. Alzubadi, Indian J. Phys. **89**, 619 (2015). https://doi.org/10.1007/s12648-014-0614-3
[16] P.-G Reinhard, B. Schuetrumpf, J.A. Maruhn, "The Axial Hartree–Fock + BCS Code SkyAx," Comp. Phys. Comm. **258**, 107603 (2021). https://doi.org/10.1016/j.cpc.2020.107603
[17] B.A. Brown, and W.D.M. Rae, Nucl. Data Sheets, **120**, 115 (2014). https://doi.org/10.1016/j.nds.2014.07.022
[18] A. Magilligan, and B.A. Brown, "New isospin-breaking "USD" Hamiltonians for the sd shell," Phys. Rev. C, **101**, 064312 (2020). https://doi.org/10.1103/PhysRevC.101.064312
[19] National Nuclear Data Center (NNDC), Brookhaven National Laboratory, Upton, NY, 11973-5000, http://www.nndc.bnl.gov/
[20] B. Pritychenko. M. Birch, B. Singh, and M. Horoi, Atom. Data Nucl. Data Tab. **107**, 1 (2016). https://doi.org/10.1016/j.adt.2015.10.001

[21] W.A. Richter, S. Mkhize, and B.A. Brown, Phys. Rev. C, **78**, 064302 (2008). https://doi.org/10.1103/PhysRevC.78.064302
[22] S. Mitsunobu, and Y. Torizuka, Phys. Rev. Lett. **28**, 920 (1972). https://doi.org/10.1103/PhysRevLett.28.920
[23] X.K. Maruyama, F.J. Kline, J.W. Lightbody, Jr., S. Penner, W.J. Briscoe, M. Lunnon, and H. Crannell, Phys. Rev. C, **19**, 1624 (1979). https://doi.org/10.1103/PhysRevC.19.1624
[24] A.I. Steshenko, Nucl. Phys. A, **445,** 462 (1985). https://doi.org/10.1016/0375-9474(85)90452-X
[25] A. Obertelli, and H. Sagawa, *Modern Nuclear Physics from Fundamentals to Frontiers*, (Springer Nature, Singapore, 2021).
[26] R.P Singhal, H.S. Caplan, J.R. Moreira, and T.E. Drake, Can. J. Phys. **51,** 2125 (1973). https://doi.org/10.1139/p73-278

ФОРМ-ФАКТОРИ ЕЛЕКТРОЗБУДЖЕННЯ ТА ДЕФОРМАЦІЯ ІЗОТОПІВ ^{20,22}NE НА ОСНОВІ МОДЕЛІ ОБОЛОНКИ ТА РОЗРАХУНКІВ HARTREE-FOCK PLUS BCS

Омар А. Алсвайдаві, Алі А. Альзубаді
Факультет фізики, Науковий коледж, Багдадський університет, Багдад, Ірак

За допомогою оболонкової моделі з розрахунками Скірма-Хартрі-Фока досліджено ядерну структуру ізотопів ^{20,22}Ne. Зокрема, були досліджені переходи до збуджених станів низького рівня позитивної та негативної парності в трьох моделях оболонок; sd для позитивних станів парності, *spsdpf* з великим базисом (без ядра) та простори моделі *zbme* для станів з негативною парністю. Оцінено енергії збудження, зменшені ймовірності переходу, пружні та непружні форм-фактори та порівняно з наявними експериментальними даними. Взаємодія Скірма була використана для створення потенціалу одного тіла в розрахунках Хартрі-Фока для кожного вибраного збудженого стану, який потім використовується для розрахунку одночастинкових матричних елементів. Взаємодія Скірма була використана для розрахунку радіальних хвильових функцій одночастинкових матричних елементів, з яких може бути згенерований потенціал одного тіла в теорії Хартрі-Фока з параметризацією SLy4. Крім того, ми дослідили взаємодію між профілями густини нейтронів і протонів у двох вимірах разом із деформаціями ^{20,22}Ne за допомогою розрахунків Хартрі-Фока та BCS.

Ключові слова: *Sd модельний простір; стан негативного паритету; пружний і нееластичний форм-фактор; розподіл щільності*